Loss of phosphatidylinositol-4-phosphate 5-kinase type-1 gamma (Pip5k1c) in mesenchymal stem cells leads to osteopenia by impairing bone remodeling

Qinnan Yan[1,‡], Huanqing Gao[1,‡], Qing Yao[1], Kun Ling[2], and Guozhi Xiao[1,*]

From the [1]Department of Biochemistry, School of Medicine, Southern University of Science and Technology, Guangdong Provincial Key Laboratory of Cell Microenvironment and Disease Research, Shenzhen Key Laboratory of Cell Microenvironment, Shenzhen, China; [2]Department of Biochemistry and Molecular Biology, Mayo Clinic, Rochester, Minnesota, USA

Edited by Roger Colbran

Phosphatidylinositol-4-phosphate 5-kinase type-1 gamma (Pip5k1c) is a lipid kinase that plays a pivotal role in the regulation of receptor-mediated calcium signaling in multiple tissues; however, its role in the skeleton is not clear. Here, we show that while deleting Pip5k1c expression in the mesenchymal stem cells using Prx1-Cre transgenic mice does not impair the intramembranous and endochondral ossification during skeletal development, it does cause osteopenia in adult mice, but not rapidly growing young mice. We found Pip5k1c loss dramatically decreases osteoblast formation and osteoid and mineral deposition, leading to reduced bone formation. Furthermore, Pip5k1c loss inhibits osteoblastic, but promotes adipogenic, differentiation of bone marrow stromal cells. Pip5k1c deficiency also impairs cytoplasmic calcium influx and inactivates the calcium/calmodulin-dependent protein kinase, which regulates levels of transcription factor Runx2 by modulating its stability and subsequent osteoblast and bone formation. In addition, Pip5k1c loss reduces levels of the receptor activator of nuclear factor-κB ligand, but not that of osteoprotegerin, its decoy receptor, in osteoblasts in bone and in sera. Finally, we found Pip5k1c loss impairs the ability of bone marrow stromal cells to support osteoclast formation of bone marrow monocytes and reduces the osteoclast precursor population in bone marrow, resulting in reduced osteoclast formation and bone resorption. We conclude Pip5k1c deficiency causes a low-turnover osteopenia in mice, with impairment of bone formation being greater than that of bone resorption. Collectively, we uncover a novel function and mechanism of Pip5k1c in the control of bone mass and identify a potential therapeutic target for osteoporosis.

Inositol 1,4,5 trisphosphate (IP3) generated by the hydrolysis of PIP2 is an inositol phosphate signaling molecule that is involved in the regulation of intracellular calcium concentration. Type 1 phosphatidylinositol 4-phosphate 5-kinases (Pip5k1s) generate PIP2 by phosphorylating the five position on the inositol ring of phosphatidylinositol 4-phosphate. In mammalian cells, there are three isoforms of Pip5k1 proteins (Pip5k1a, Pip5k1b, and Pip5k1c) (1). Previous studies have demonstrated that Pip5k1c regulates receptor-mediated calcium signaling, actin cytoskeletal dynamics, endocytosis, and exocytosis (2–11). $Pip5k1c^{-/-}$ mice have 50% less PIP2 in their brains and die within 24 h after birth (2). Zhu et al. reported that Pip5k1c is important for osteoclast function (12). However, the role of Pip5k1c in skeletal development and homeostasis remains unknown.

Bone is a dynamic tissue with constant remodeling (13), which comprises two processes: bone resorption and bone formation. Bone resorption is controlled by osteoclasts which remove the aged or damaged bone, thus forming resorption cavities. Osteoblasts arrive at the cavities where that secrete molecules filling in the pit and form new bone. Bone resorption and formation are spatially and temporally coupled and delicately balanced. Imbalance between bone resorption and formation leads to metabolic bone diseases, such as osteopenia or osteopetrosis. Defects in osteoblast generation or activity can result in reduced bone mass or osteopenia. Osteoblasts are differentiated from the mesenchymal stem cells (MSCs) (14, 15). Several key transcription factors and signaling pathways are involved in control of differentiation of MSCs toward the osteoblastic cells (15–17). Runx2 is an important transcription factor essential for osteoblast formation and differentiation. While it is known that expression and activity of Runx2 can be modulated at both the transcriptional and posttranslational mechanisms (18), upstream signals that modulate Runx2 are incompletely understood.

The aim of this study was to determine whether Pip5k1c plays a role in skeletal development and homeostasis and, if so, what the underlying mechanism(s) are. We demonstrate that Pip5k1c loss in MSC causes a low-turnover osteopenia in adult mice. Mechanistically, Pip5k1c loss inactivates calcium/calmodulin-dependent protein kinase (CaMK) and downregulates the level of Runx2 protein, leading to inhibition of osteoblast and bone formation. In the meantime, Pip5k1c loss reduces osteoclast precursor population and expression of receptor activator of nuclear factor-κB ligand (Rankl) to inhibit

---

‡ These authors contributed equally to this work.
* For correspondence: Guozhi Xiao, xiaogz@sustech.edu.cn.

osteoblastic support of osteoclast formation, thus impairing bone resorption.

Results

Deleting Pip5k1c expression in the limb and head MSCs does not markedly alter the skeletal development in mice

Previous studies have reported that the conventional PIPKIγ (*i.e.,* Pip5k1c) knockout is lethal (2, 10), which prevents us from investigating its postnatal role in organ formation and homeostasis. In this study, we constructed a Pip5k1c conditional knockout mouse line as described in Experimental procedures. To investigate the role of Pip5k1c in skeletal development, we generated mice with deletion of Pip5k1c expression in the limb and head MSC by breeding the *Prx1-Cre* transgenic mice (19) and floxed *Pip5k1c* mice (*Pip5k1c^{fl/fl}*). Genotypes of the mutant mice were determined by PCR analysis with tail genomic DNA (Fig. 1*A*). The Cre-negative *Pip5k1c^{fl/fl}* mice were used as control mice (referred to as WT hereafter) in this study. cKO mice were born at the expected Mendelian frequency. Results from quantitative real-time RT-PCR analysis of total RNA isolated from the indicated tissues of E14.5 control and cKO mice showed that the level of *Pip5k1c* mRNA was dramatically decreased in forelimb, but not in lung, liver, heart, and brain, in cKO mice relative to that in control mice (Fig. 1*B*). At P0, cKO mice did not display any marked abnormalities in the gross appearance and body weight compared to their control littermates (Fig. 1, *C* and *D*). Alizarin red and alcian blue double staining of whole-mount skeletons revealed no marked abnormalities in the skull vault, forelimb, hindlimb, clavicle, rib cage, and sterna in cKO mice (Fig. 1, *E–G*). Quantitative analyses indicated that the lengths of all the long bones (femur, tibia, humerus, radius, and ulna) and their respective bony portions stained red by alizarin red were not significantly different between the two genotypes (Fig. 1*G*). The formation of primary ossification center is a key process during the endochondral ossification, and its length was not significantly different in WT and cKO mice (P0) (Fig. 1, *H* and *I*). In the humeral growth plate, the chondrocytes in the proliferation zone were arranged into regular columns in both control and cKO mice (P0), and the hypertrophic chondrocytes in the hypertrophic zone had similar size in the two genotypes (Fig. 1*J*). Alcian blue staining of the tibial sections from P17 mice showed that the secondary ossification center was similarly formed in control and cKO mice (Fig. 1*K*). Collectively, these results suggest that Pip5k1c deletion does not impact both the endochondral and intramembranous ossification during early skeletal development.

Pip5k1c deletion causes a low bone mass phenotype in adult mice but not in rapidly growing young mice

We observed a slight reduction in body weight in the 4-month-old cKO mice relative to control littermates (Fig. 2*A*). While at this time the lengths of femurs were not significantly different between the two genotypes (Fig. 2, *B* and *C*), results from H/E staining of tibial sections revealed markedly reduced trabecular bone mass in cKO mice compared to their control

littermates (Fig. 2*D*). Growth plate widths were not significantly altered by Pip5k1c deletion (Fig. 2*E*). Microcomputed tomography (μCT) analyses of the distal femur of 4-month-old male cKO mice displayed a significant bone loss both in trabecular bone compared with their sex-matched control littermates (Fig. 2*F*). The bone mineral density (BMD) (Fig. 2*G*), bone volume/tissue volume fraction (BV/TV) (Fig. 2*H*), and trabecular number (Tb.N) (Fig. 2*I*) were all significantly decreased in cKO mice compared with those in control littermates. Pip5k1c deletion did not markedly alter the trabecular separation (Tb.Sp) (Fig. 2*J*), trabecular thickness (Tb.Th) (Fig. 2*K*), cortical thickness (Fig. 2*L*), cortical area (Fig. 2*M*), and marrow area (Fig. 2*N*). A similar osteopenia was observed in 4-month-old female cKO mice (data not shown). It should be noted that this osteopenic phenotype was not observed in 1-month-old cKO male and female mice (data not shown). Furthermore, μCT analysis from skull vault showed a comparable BMD, BV/TV, Tb.N, Tb.Sp, and Tb.Th in control and cKO mice (Fig. 2, *O–T*). To examine any possible differences in calvarial structure, we compared the μCT coronal sections of calvariae at the interphase (indicated by *red arrow* in Fig. 2*O*) between parietal and interparietal bones in control and cKO mice (Fig. 2*U*). Superimposed images from control (in *blue*) and cKO (in *pink*) revealed that the coronal section structures of calvariae were not different between the two mice (Fig. 2*V*). Results from μCT analyses revealed no marked alterations in the spinal vertebral body bone (Fig. 2*W*) and alveolar bone (Fig. 2*X*) difference between the two genotypes at 4 months of age.

Pip5k1c deletion severely impairs osteoblast formation, osteoid and mineral production, and bone formation *in vivo*

To investigate mechanism(s) underlying the osteopenic phenotype in cKO mice, we determined whether Pip5k1c loss impairs the osteoblast formation and function. Results from ELISA assay revealed that the level of the serum procollagen type 1 amino terminal propeptide (P1NP), an indicator of *in vivo* osteoblast function and bone formation, was significantly reduced in 4-month-old cKO mice relative to that in control littermates (Fig. 3*A*). Results from the calcein double labeling experiments showed that the *in vivo* osteoblast bone-forming activity was decreased by Pip5k1c deletion. The mineral apposition rate (MAR), mineralizing surface per bone surface (MS/BS), and bone formation rate (BFR) were reduced in both the femoral metaphyseal cancellous and diaphyseal cortical bones in 4-month-old cKO mice compared with those in control littermates (Fig. 3, *B–E*). Analyses of the Masson staining of the undecalcified femoral sections indicated that the osteoid volume/bone volume was dramatically decreased in cKO mice compared with that in control littermates (Fig. 3, *F* and *G*). The results of immunohistochemical (IHC) staining displayed that the numbers of osterix (Osx)-expressing cells (*i.e.,* osteoblasts and osteoprogenitors) located on the tibial metaphyseal cancellous bone surface were drastically decreased in cKO mice compared with those in control littermates (Fig. 3, *H* and *I*).
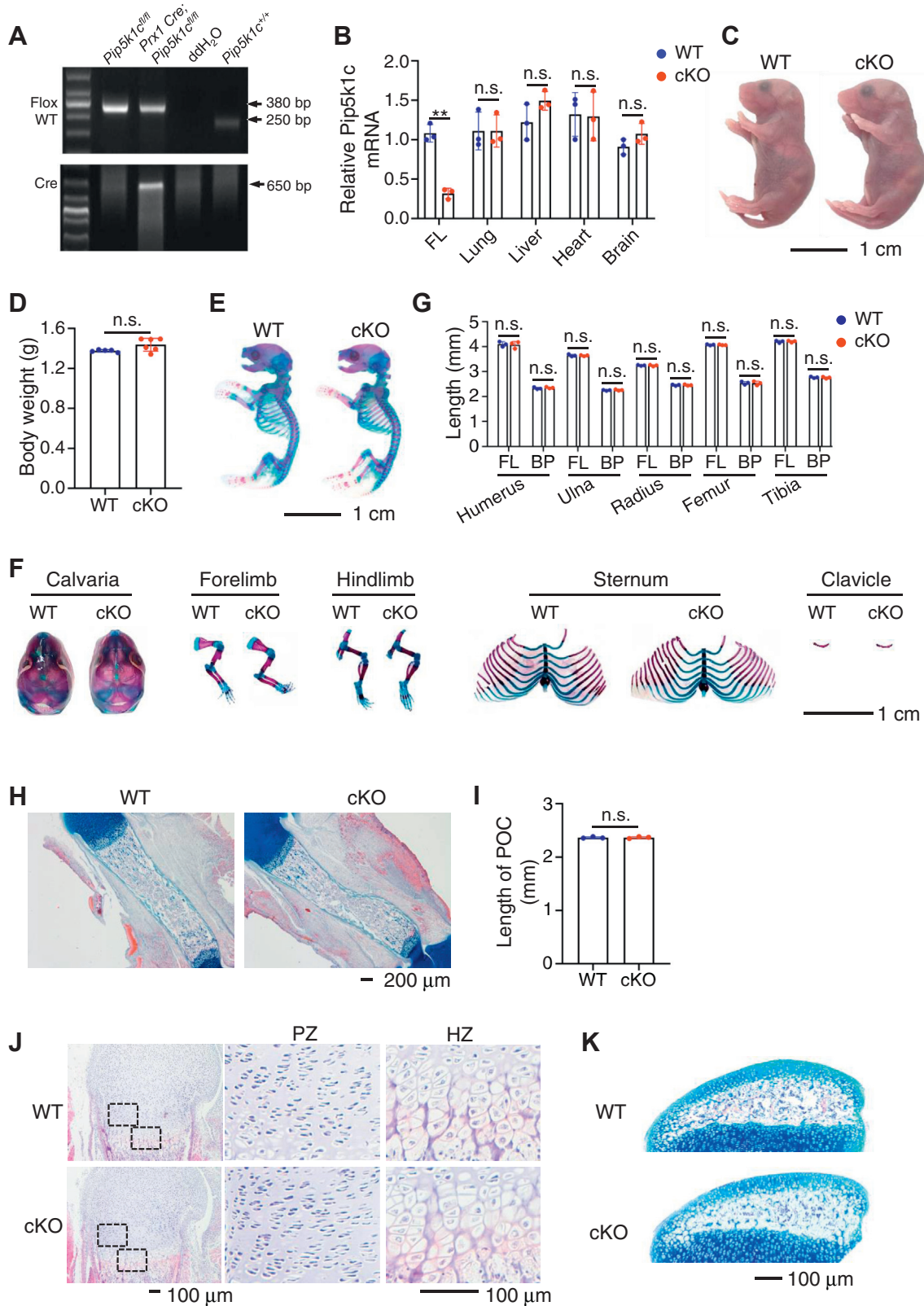
Figure 1. Deletion of Pip5k1c in limb and head mesenchymal stem cells does not affect skeletal development in mice. *A,* genotyping. Representative PCR analysis of genomic DNA extracted from tail clippings. PCR product bands of floxed (380 bp) and control (WT) (250 bp) are shown. Cre PCR product band (650 bp) is indicated. *B,* real-time quantitative reverse transcription PCR (qRT-PCR) analysis. Total RNA isolated from the indicated tissues of E14.5 *Pip5k1c*[Prx1]cKO (cKO) or Cre-negative *Pip5k1c*^{fl/fl} (WT) littermates were subjected to qRT-PCR analysis for *Pip5k1c* expression. FL, forelimb. *Pip5k1c* mRNA was normalized to *Gapdh* mRNA. Results were expressed as mean ± standard deviation (SD); $N = 3$ mice per group. **$p < 0.01$ *versus* control; Unpaired two-tailed *t* test. *C,* gross appearance of P0 control and cKO mice. Scale bar, 1 cm. *D,* body weight of P0 control and cKO mice. Results were expressed as mean ± SD; $N = 5$ mice for control, $N = 6$ mice for cKO. n.s., not significant; Unpaired two-tailed *t* test. *E,* alizarin red and alcian blue double staining of P0 control and cKO skeletons. Scale bar, 1 cm. *F,* calvaria, forelimb, hindlimb, sternum, and clavicle from P0 control and cKO mice. Scale bar, 1 cm. *G,* quantitative data of

Pip5k1c deletion decreases the formation of the colony forming unit-fibroblast and colony forming unit-osteoblast and osteoblast differentiation and increases adipogenic differentiation of the bone marrow stromal cells *in vitro*

To explore possible mechanism(s) for reduced osteoblast formation in cKO mice, we performed the colony forming unit-fibroblast (CFU-F) assays and colony forming unit-osteoblast (CFU-OB) assays using primary bone marrow (BM) cells from 4-month-old cKO and control littermates. The results showed that the numbers of CFU-F (Fig. 4, *A* and *B*) and CFU-OB colonies (Fig. 4, *C* and *D*) were reduced by 46% and 41%, respectively, in cKO group relative to those in control group. We examined the *in vitro* differentiation capacity of primary bone marrow stromal cells (BMSCs) from the two genotypes and found that the mineralization and osteoblast gene expression were both decreased in cKO group compared with those control group (Fig. 4, *E* and *F*). In contrast, the adipogenic differentiation capacity of BMSC from cKO mice was increased compared to that in control group. The adipocyte formation and adipocyte gene expression were both increased in cKO group compared with those in control group (Fig. 4, *G* and *H*). *In vivo*, a dramatic increase in adiposity was observed in the BM of distal tibiae in cKO mice relative to that in control littermates (Fig. 4*I*).

Pip5k1c loss decreases the level of Runx2 protein by impairing cytoplasmic Ca²⁺ levels and CaMK activation in BMSC

Previous studies have shown that Pip5k1c regulates the levels of intracellular Ca^{2+} (9, 11). Pip5k1c generates PIP2 by phosphorylating the five position on the inositol ring of phosphatidylinositol 4-phosphate [PI(4)P] (20). PIP2 hydrolysis produces diacylglycerol and IP3. IP3 can bind to IP3 receptor in the endoplasmic reticulum (ER), which will lead to the Ca^{2+} release from endoplasmic reticulum to cytosol. Thus, we next determined whether Pip5k1c knockdown (KD) by siRNA affects the intracellular Ca^{2+} levels traced by fluo-4/AM, a probe for cytoplasmic Ca^{2+}. As expected, the fluorescence intensity was decreased in BMSCs with Pip5k1c KD compared to that in BMSCs treated with control siRNA (si-NC) (Fig. 5, *A* and *B*). Western blotting results showed that the protein level of Runx2 was reduced by Pip5k1c KD (Fig. 5, *C* and *D*). However, the mRNA level of Runx2 was not significantly altered by Pip5k1c KD (Fig. 5*E*), suggesting that a mechanism of posttranscriptional regulation is involved. The protein level of phosphorylated CaMK2 (p-CaMK2), but not its total CaMK2 protein, was decreased by Pip5k1c KD (Fig. 5, *C* and *D*). Pip5k1c KD did not markedly impact the expression levels of p-Erk, total Erk, active β-catenin, total β-catenin, p-Creb, and total Creb proteins in primary BMSCs (Fig. 5, *F* and *G*). Furthermore, IHC staining for the tibial sections showed that Runx2 expression was decreased in osteoblasts from cKO

mice compared with that in control littermates (Fig. 5, *H* and *I*). The expression level of osteocalcin (Ocn), a well-known Runx2 downstream target, was drastically reduced in osteoblasts located on the bone surfaces in cKO mice (Fig. 5, *J* and *K*). We next performed experiments to explore how p-CaMK2α modulates Runx2. First, we co-transfected COS-7 cells with Runx2 expression plasmid together with increasing concentrations of a kinase-dead form of CaMK2α (KD-CaMK2α) or a constitutively active form of CaMK2α (CA-CaMK2α) expression plasmids for 24 h and found that CA-CaMK2α, but not kinase-dead form of CaMK2α (KD-CaMK2α), increased the level of Runx2 in a dose-dependent manner (Fig. 5, *L–O*). We further determined whether CA-CaMK2α can stabilize Runx2 protein. In the presence of cycloheximide, which blocks the *de novo* protein synthesis, overexpression of CA-CaMK2α delayed the degradation of Runx2 protein (Fig. 5, *P* and *Q*).

Decreased osteoclast formation and bone resorption in cKO mice

Bone mass is delicately regulated by not only the osteoblast-mediated bone formation, but also the osteoclast through bone resorption. We further investigated whether Pip5k1c loss impacts osteoclast formation and bone resorption by performing several experiments. First, results from ELISA assays of the sera from the two genotypes revealed a significant reduction of the collagen type 1 cross-linked C-telopeptide (CTX-1), an *in vivo* bone resorption marker, in cKO *versus* control littermates (Fig. 6*A*). Second, we evaluated the *in vivo* osteoclast formation by performing the tartrate-resistant acid phosphatase (TRAP) staining of the decalcified tibial sections of control and cKO mice (Fig. 6*B*). The results showed that the osteoclast surface/bone surface (Fig. 6*C*) and osteoclast number/bone perimeter (Fig. 6*D*) in both the primary and secondary spongiosa were decreased in cKO mice compared with those in control littermates. Third, results from *in vitro* osteoclast formation assays showed that fewer multinucleated TRAP positive osteoclasts were formed in primary bone marrow monocytes (BMMs) from cKO mice than from control littermates (Fig. 6*E*). The number of TRAP positive multinucleated cells (MNCs, defined as having three or more nuclei per cell) in cKO BMM cultures was reduced by about 50% relative to that in control BMM cultures (Fig. 6*F*).

Reduced osteoclast precursor population in the BM of cKO mice

It is known that cells with CD3⁻ CD45R⁻ CD11b⁻/low CD117⁺ CD115hi in BM have the highest ability to differentiate into osteoclasts *in vitro* (21). We determined whether the Pip5k1c loss affects this osteoclast precursor population in BM by flow cytometry analysis and found that this cell population

---

full-length (FL) and bony portion length of the indicated bones from (*E*). Results were expressed as mean ± SD; *N* = 3 mice per group. Unpaired two-tailed *t* test. *H*, alcian blue staining of femur sections from P0 control and cKO mice. Scale bar, 200 μm. *I*, quantitative data from (*H*). Results were expressed as mean ± SD; *N* = 3 mice per group. n.s., not significant; unpaired two-tailed *t* test. *J*, H/E staining of P0 control and cKO femur sections. Representative images of proliferation zone (PZ) and hypertrophic zone (HZ) from P0 control and cKO femurs. Scale bar, 100 μm. *K*, alcian blue staining of P17 control and cKO tibiae. The secondary ossification centers are shown. Scale bar, 100 μm. BP, bony portion; n.s., not significant; PZ, proliferation zone; HZ, hypertrophic zone.
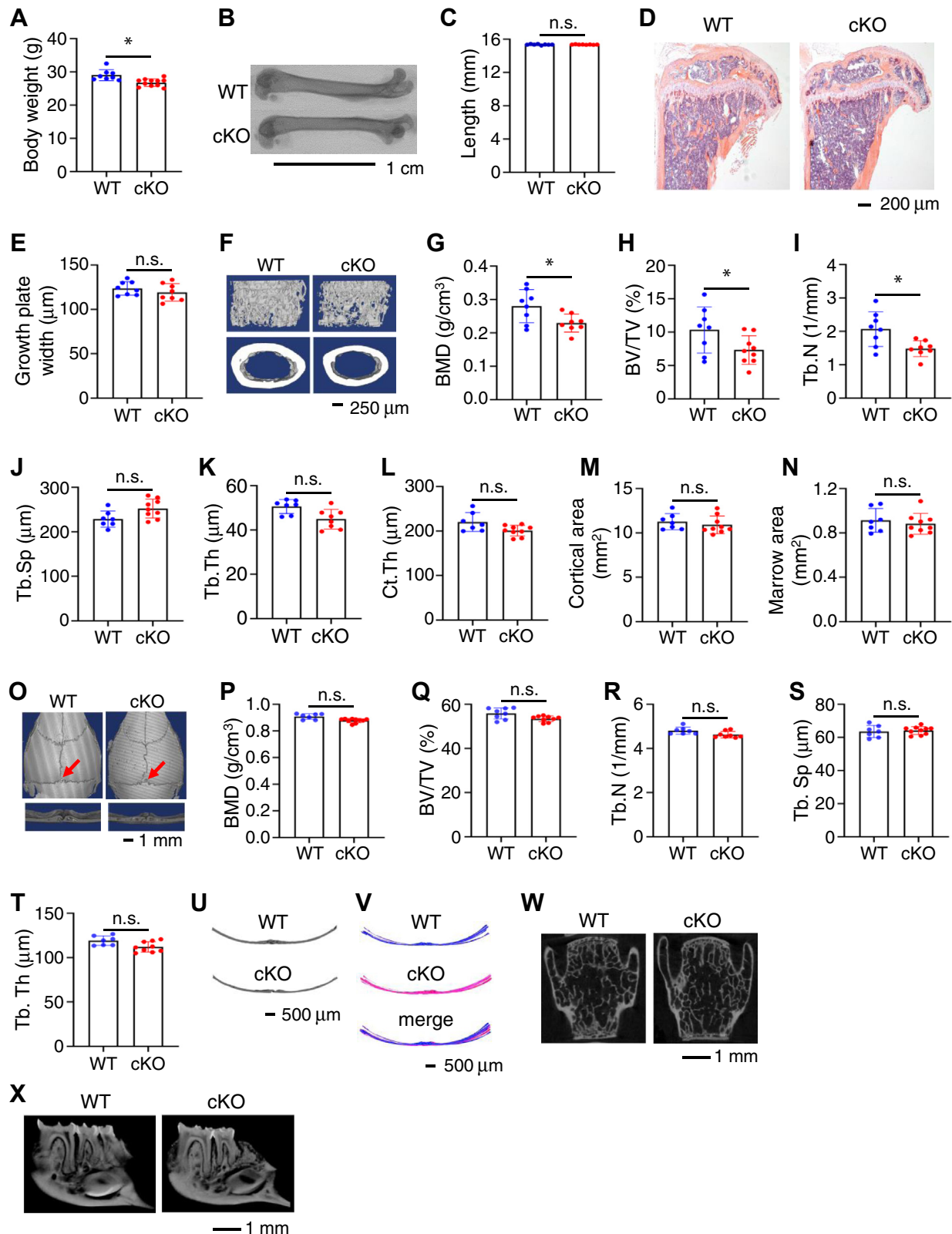
Figure 2. *Pip5k1c^Prx1* cKO mice display low bone mass at adult stage. *A*, body weight of 4-month-old male mice. Results were expressed as mean ± SD; *N* = 8 mice for control, *N* = 11 mice for cKO. **p* < 0.05, *versus* WT; unpaired two-tailed *t* test. *B* and *C*, gross appearance of femurs from 4-month-old male mice scanned by microcomputerized tomography (*B*), and the femur lengths were measured (*C*). Scale bar, 1 cm. Results were expressed as mean ± SD; *N* = 8 mice for each group. n.s., not significant; unpaired two-tailed *t* test. *D*, H/E staining of tibial sections from 4-month-old male mice. Scale bar, 200 μm. *E*, growth plate widths were measured based on the H/E staining of tibial sections from 4-month-old male mice. Results were expressed as mean ± SD; *N* = 8 mice for each group. n.s., not significant; unpaired two-tailed *t* test. *F*, three-dimensional (3D) reconstruction from microcomputerized tomography scans of distal femurs from 4-month-old male control and cKO mice. Scale bar, 250 μm. *G–N*, quantitative analyses of the bone mineral density (*G*), bone volume/ tissue volume (*H*), and trabecular number (*I*), trabecular separation (*J*), trabecular thickness (*K*), cortical thickness (Ct.Th) (*L*), cortical area (*M*), and marrow
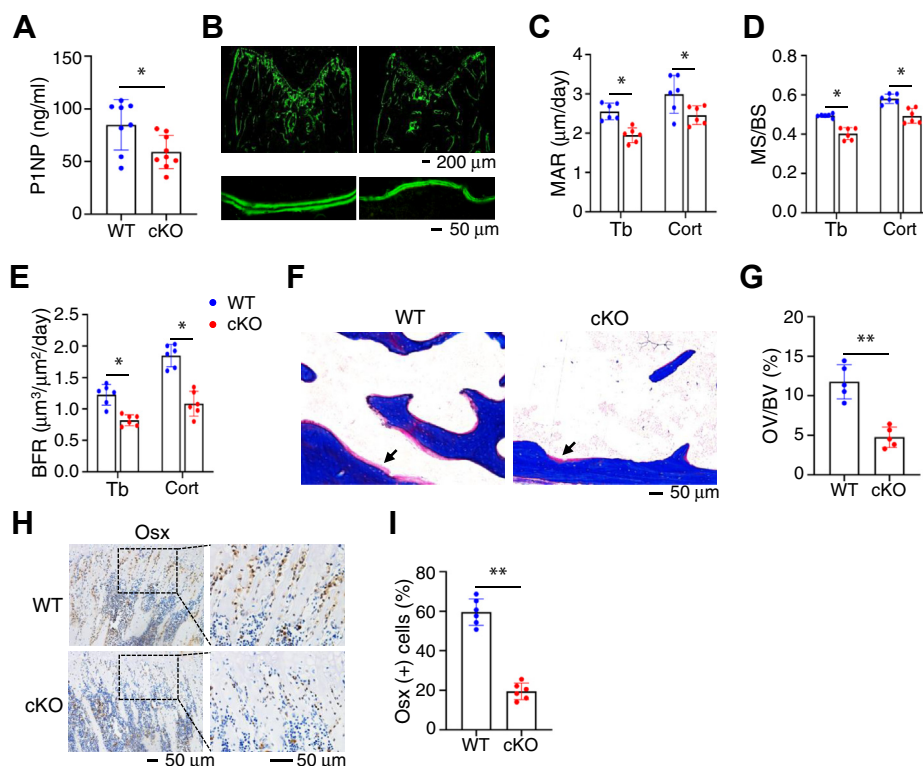
Figure 3. Pip5k1c loss impairs bone formation, osteoid deposition, and osteoblast numbers in bone. *A*, serum levels of procollagen type 1 amino-terminal propeptide (P1NP) from 4-month-old control and cKO male mice. Results were expressed as mean ± SD; $N = 7$ mice for control, $N = 9$ mice for cKO. *$p < 0.05$ *versus* control; unpaired two-tailed *t* test. *B-E*, calcein double labeling. Representative images of 4-month-old control and cKO femur sections (*B*). Scale bar, 50 µm. Quantitative analyses of the mineral apposition rate (*C*), mineralizing surface per bone surface (*D*), and bone formation rate (*E*) of trabecular bone and cortical bone from (*B*). Results were expressed as mean ± SD; $N = 6$ mice per group from 4-month-old male mice. *$p < 0.05$ *versus* control; unpaired two-tailed *t* test. *F,* Masson staining of undecalcified femur sections from 4-month-old male control and cKO mice. *G,* quantification of the osteoid volume to bone volume from (*F*). Results were expressed as mean ± SD; $N = 5$ mice per group. **$p < 0.01$ *versus* control; unpaired two-tailed *t* test. *H* and *I*, immunohistochemical (IHC) staining. Tibial sections of 4-month-old control and cKO mice were subjected to IHC staining for expression of osterix. Scale bar, 50 µm. Quantification of (*H*). Results were expressed as mean ± SD; $N = 6$ mice per group. **$p < 0.01$ *versus* control; Unpaired two-tailed *t* test. P1NP, procollagen type 1 amino terminal propeptide; MAR, mineral apposition rate; MS/BS, mineralizing surface per bone surface; BFR, bone formation rate; Tb, trabecular bone; Cort, cortical bone; OV/BV, osteoid volume to bone volume; Osx, osterix.

was significantly reduced in cKO mice compared with that in control littermates (Fig. 6, *G* and *H*).

### BMSCs from cKO mice fail to efficiently support osteoclast formation

To further explore how osteoclast formation is impaired in cKO mice, we next conducted the co-culture experiments to investigate whether BMSCs from cKO mice could normally support osteoclast formation of cKO BMM in BMSC/BMM co-cultures (Fig. 6, *I* and *J*). As expected, co-cultures of WT BMSC with WT BMM induced formation of a number of TRAP⁺ MNC. The number of TRAP⁺ MNC was drastically reduced in WT BMSC/cKO BMM co-cultures, when compared with that of WT BMSC/WT BMM co-cultures. This result suggests an intrinsic defect in osteoclast formation in cKO BMM. Furthermore, the number of TRAP⁺ MNC was significantly decreased in the cKO BMSC/WT BMM co-

cultures, compared to that in WT BMSC/WT BMM, suggesting that the ability of cKO BMSC to support osteoclast formation is impaired by Pip5k1c deletion.

Pip5k1c loss reduces Rankl expression in BMSC and osteoblasts

Rankl and osteoprotegerin (Opg) are both key factors that regulate osteoclast formation and differentiation. We further determined their serum levels in the two phenotypes by ELISA assays and found that Rankl level in cKO sera was significantly decreased compared to that in control sera (Fig. 6*K*). However, the serum levels of Opg, which is a decoy receptor of Rankl and inhibits osteoclast formation, were not significantly different between the two groups (Fig. 6*L*). Thus, the Rankl/Opg ratio was reduced in cKO *versus* control littermates (Fig. 6*M*). Results from IHC staining revealed a dramatic reduction in

area (*N*) of distal femurs from (*F*). Results were expressed as mean ± SD; $N = 8$ mice for control, $N = 9$ mice for cKO. *$p < 0.05$ *versus* control; Unpaired two-tailed *t* test. (*O*) Three-dimensional (3D) reconstruction from µCT scans of skull from 4-month-old male control and cKO male mice. Scale bar, 1 mm. *P–T*, quantitative analyses of the bone mineral density (*P*), bone volume/tissue volume (BV/TV) (*Q*), and trabecular number (*R*), trabecular separation (*S*), trabecular thickness (*T*) of skull from (*O*). Results were expressed as mean ± SD; $N = 8$ mice for control, $N = 9$ mice for cKO. n.s., not significant; Unpaired two-tailed *t* test. *U,* µCT cross-section view of the suture of parietal and interparietal bones. *V,* superimposed cross-section image results for eight control mice and 10 cKO mice. *W* and *X,* µCT scans of L4 spinal vertebral body bone (*W*) and alveolar bone (*X*) from 4-month-old control and cKO male mice. Scale bar, 1 mm. Tb.N, trabecular number; Tb.Sp, trabecular separation; Tb.Th, trabecular thickness; BMD, bone mineral density; Ct.Th, cortical thickness.
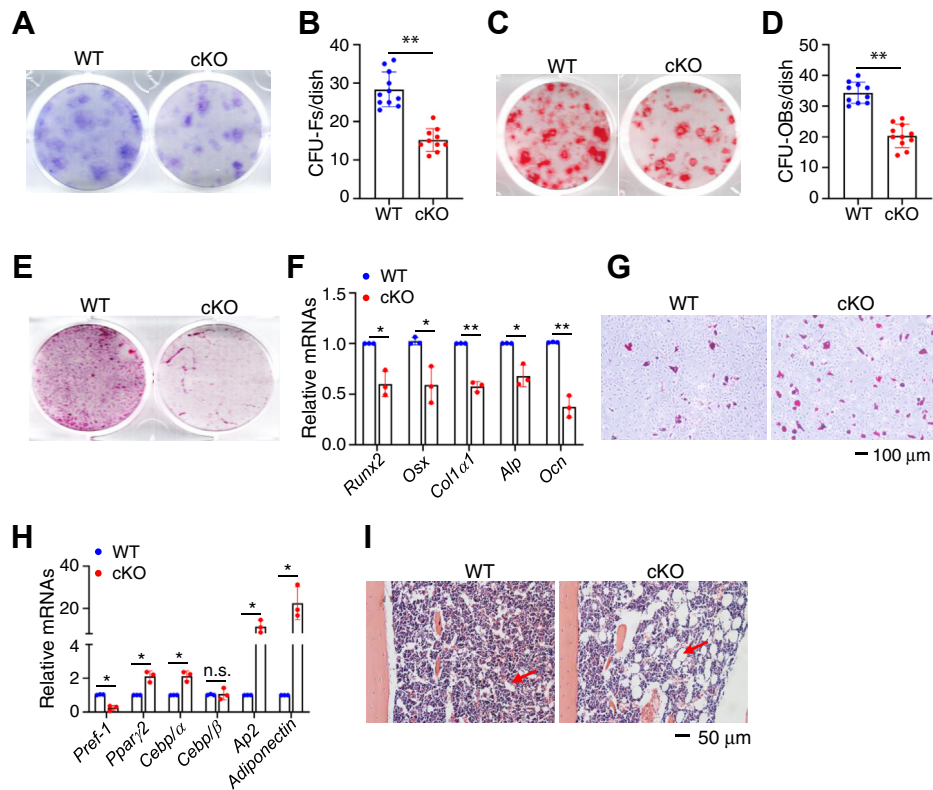
Figure 4. Pip5k1c loss impairs osteoblast, but promotes adipogenic, formation and differentiation. *A,* colony forming unit-fibroblast (CFU-F) assays. *B,* the number of CFU-F was counted under a microscope. Results were expressed as mean ± SD; *N* = 11 mice for control, *N* = 10 mice for cKO. **p < 0.01 *versus* control; Unpaired two-tailed *t* test. *C,* colony forming unit-osteoblast (CFU-OB) assays. *D,* the number of CFU-OB was counted under a microscope. Results were expressed as mean ± SD; *N* = 10 mice for control, *N* = 11 mice for cKO. **p < 0.01 *versus* control; unpaired two-tailed *t* test. *E* and *F,* primary BMSC isolated from 4-month-old control and cKO male mice and cultured with osteoblast differentiation medium for 14 days, followed by alizarin red staining (*E*) and RT-qPCR analyses (*F*). Results were expressed as mean ± SD; *N* = 3 biologically independent experiments. *p < 0.05, **p < 0.01 *versus* control; unpaired two-tailed *t* test. *G* and *H,* primary BMSCs isolated from 4-month-old control, and cKO male mice were cultured with adipogenic medium for 14 days, followed by Oil Red O staining (*G*) and RT-qPCR analyses (*H*). Results were expressed as mean ± SD; *N* = 3 biologically independent experiments. *p < 0.05, *versus* control; unpaired two-tailed *t* test. *I,* bone marrow adiposity. Tibial sections of 4-month-old control, and cKO male mice were subjected to H/E staining. BMSCs, bone marrow stromal cells. Runx2, Runt-related transcription factor 2; Osx, Osterix; Col1a1, type 1 collagen a1; Alp, alkaline phosphatase; Ocn, Osteocalcin; Pref-1, preadipocyte factor 1; Pparg2, peroxisome proliferator-activated receptor gamma 2; Cebp/α, CCAAT/enhancer-binding protein (C/EBP), alpha; Cebp/β, CCAAT/enhancer-binding protein (C/EBP), beta; Ap2, adipocyte protein 2.

expression of Rankl protein in osteoblasts on cKO tibial surfaces compared to that in control group (Fig. 6, *N* and *O*).

Discussion

In this study, by using cellular and biochemical approaches and genetic mouse model, we demonstrate that Pip5k1c deficiency in MSC causes an osteopenia in adults but not in rapidly growing young mice. Notably, the deletion of Pip5k1c in MSC does not impair the intramembranous and endochondral ossification during skeletal development. We demonstrate that the loss of Pip5k1c in MSC causes a low-turnover osteopenia in mice, in which impairments of osteoblast and bone formation are greater than those of osteoclast formation and bone resorption.

We demonstrate that Pip5k1c expression in MSC is essential for osteoblast formation in bone. Pip5k1c loss largely reduces the formation of osteoblastic cells in the BM and on the bone surfaces. This is achieved partly by downregulation of transcription factor Runx2. The expression of Runx2 protein, but not its mRNA, is dramatically decreased in BMSC and osteoblast in cKO mice. We further demonstrate that Pip5k1c

loss downregulates Runx2 protein by inactivating CaMK2 in BMSC. Previous studies from our and other groups have demonstrated that expression and activity of Runx2 can be modulated by multiple factors, key signaling pathways, such as ERK/MAPK, p38 and PKA, and microRNAs (18, 22). In this study, we demonstrate that the level of Runx2 protein is regulated by the Pip5k1c-CaMK2 signaling in MSC and osteoblast, thus providing a novel knowledge regarding the regulation of Runx2 and its role in control of bone mass. It should be pointed out that while our result show that overexpression of the CA and KD CaMK2α isoforms regulates the level of Runx2 protein, these results do not exclude the possibility that other CaMK isoforms are involved in this regulation.

We demonstrate that Pip5k1c loss in MSC markedly impairs osteoclast formation and bone resorption. Our co-culture experiments reveal that BMSC from cKO mice fail to efficiently support osteoclast of the BMMs. This is partly due to reduced expression of Rankl by BMSC and osteoblast. Additionally, we find that the CD3$^-$ CD45R$^-$ CD11b$^{-/low}$ CD117$^+$ CD115^{hi} cell population (*i.e.,* osteoclast precursors) is dramatically decreased in the BM of cKO mice. Because Pip5k1c is not deleted in osteoclasts and their precursors, this
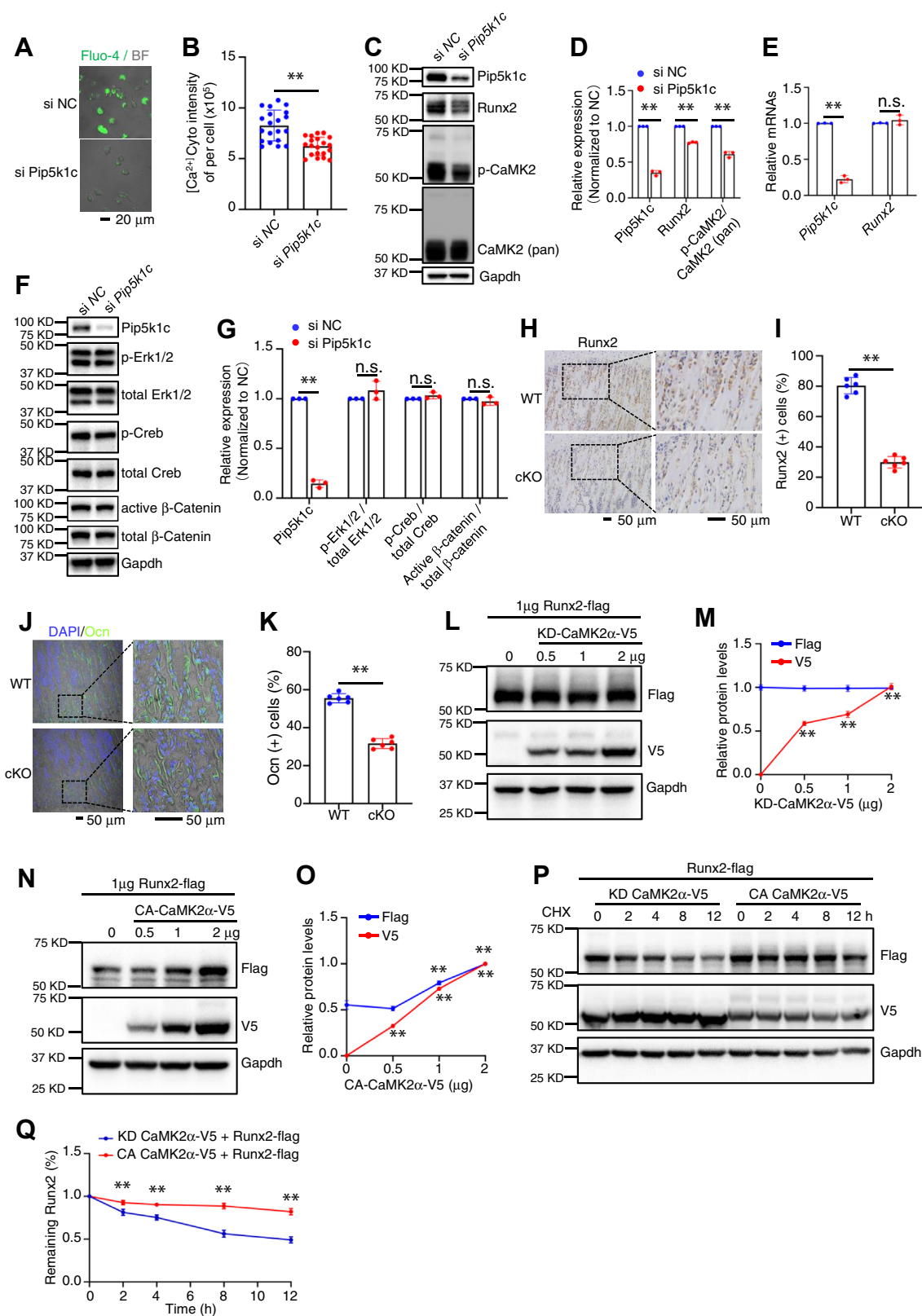
Figure 5. Pip5k1c regulates Runx2 expression through CaMK2 in BMSC. *A* and *B*, Cytosol Ca²⁺ assay. Primary BMSCs isolated from 4-month-old male mice were plated in confocal dish and knockdown (KD) of Pip5k1c by RNA interference for 48 h. Cells were then applied for Fluo-4/AM staining and signals were collected as described in Methods (*A*). Scale bar, 20 μm. The total fluorescence intensity was used as the cytoplasmic Ca²⁺ concentrations (*B*). Results were expressed as mean ± SD; N = 20 cells per group were analyzed. **p < 0.01 *versus* si-NC; unpaired two-tailed *t* test. *C–E*, primary BMSCs isolated from 4-months-old male mice were seeded in 6-well plate at 4 × 10⁵ cells per well. Pip5k1c was knocked down by RNA interference for 48 h. Protein extracts isolated from the cells were subjected to western blotting with the indicated antibodies (*C* and *D*) or RT-qPCR analysis for expression of *Pip5k1c* and *Runx2* mRNAs (*E*). Gapdh protein and mRNA were used as internal controls for Western blotting and RT-qPCR analysis, respectively. Results were expressed as mean ± SD; N = 3 biologically independent experiments. **p < 0.01 *versus* si-NC; unpaired two-tailed *t* test. *F* and *G*, primary BMSCs isolated from 4-months-

result suggests that the BM microenvironment is altered by Pip5k1c loss in MSC. The underlying mechanism(s) remain to be investigated.

It should be noted that no marked osteopenic phenotype is observed in 1-month-old cKO mice. This could be in part due to active osteoblast and bone formation and relatively less active bone-resorbing activity in rapidly growing young animals.

In summary, we define a critical role of Pip5k1c in control of bone mass, and its ablation in MSC causes a low-turnover osteopenia in mice through distinct mechanisms and provide a potential therapeutic target for osteoporosis.

Experimental procedures

Animal studies

Because the global PIPKIγ (also known as Pip5k1c) knockout is lethal (2, 10), we constructed a Pip5k1c conditional knockout mouse line. Briefly, a targeting construct was generated so that the exon two of the mouse *Pip5k1c* gene is flanked by two loxP sites and followed by a FRT site-flanked neomycin cassette before exon 3. Homologous recombination using the targeted Pip5k1c construct was performed in embryonic stem cells derived from 129 mouse substrains, and neomycin-resistant clones were selected. Recombinant embryonic stem cell clones were injected into C57BL/6 mouse embryos to generate chimeric mice. Progenies of the chimeric mice containing the targeted Pip5k1c allele were crossed with Flp recombinase transgenic mice to generate Pip5k1c loxP/wt; Flp mice, in which the neomycin cassette was removed. These animals were backcrossed with WT C57BL/6 mice six times to remove the recombinase and dilute the 129s genomic background. Pip5k1c loxP/wt mice were then self-crossed to generate Pip5k1c loxP/loxP mice (referred to as *Pip5k1c^{fl/fl}* hereafter). To generate *Prx1-Cre; Pip5k1c^{fl/fl}* mice (referred to as *Pip5k1c^{Prx1}* or cKO hereafter), *Prx1-Cre* transgenic mice (19) with Cre expression in the limb and head mesenchyme driven by the 2.4-kb *Prx1* (paired-related homeobox gene-1) gene promoter were crossed with *Pip5k1c^{fl/fl}* mice. The Cre-negative *Pip5k1c^{fl/fl}* littermates were used as control (referred to as WT) mice in this study. Mice were caged at the density of 4 to 6 mice/cage with free access to food and water. Room temperature was maintained between 20 to 24 °C. All mice were maintained in C57BL/6 background. All experimental protocols of animal studies were approved by the Institutional Animal Care and Use Committee of Southern University of Science and Technology.

Alcian blue and alizarin red S double staining of the P0 mice skeleton

The P0 mice were eviscerated and fixed in 95% ethanol for 7 days, and then the alcian blue and alizarin red S double staining was performed as we previously described (23).

μCT analysis

Fixed femurs without demineralization treatment were used for μCT analysis as we previously described, using a Bruker μCT (SkyScan 1172 Micro-CT, Bruker MicroCT) following the standards of techniques and terminology suggested by the American Society for Bone and Mineral Research (24). Briefly, femurs were scanned at 60 KV, 100 μA, 926 ms with a 10 μm voxel size. For trabecular measurements, a region of interest of 1.5 mm length starting from 0.5 mm proximal to the distal growth plate was analyzed. For cortical bone analysis, a region of interest of 1.0 mm length of mid-femoral cortical bone was analyzed. The analyses of the specimens involved the following bone measurements: the BMD, BV/TV, Tb.N, Tb.Th, Tb.Sp, cortical thickness, cortical area, and marrow area.

Bone histological evaluation

Tibias were fixed in 4% PFA overnight at 4 °C, followed by decalcification in 10% EDTA for 3 weeks as previously described (25). After decalcification, bones were embedded in paraffin and sectioned at a thickness of 5 μm used for histological evaluation.

### Calcein double labeling, MAR, MS/BS, and BFR

Calcein double labeling, MAR, MS/BS, and BFR were performed as we previously described (26). Briefly, at 7 and 2 days before sacrifice, mice were injected i.p. with calcein at a dosage of 20 mg/kg (Sigma, cat# C0875). Freshly isolated femurs were fixed in 70% ethanol and embedded with Osteo-Bed Bone Embedding kit (Sigma, cat# EM0200) following the standard protocol and sectioned at 5 μm. Images were taken using a fluorescence microscope (Olympus-BX53) and used for the evaluation of MAR, MS/BS, and BFR as we previously described (26).

CFU-F and CFU-OB assay

The CFU-F and CFU-OB assay were performed as we previously described (27). Briefly, BM nucleated cells from 4-month-old male mice were seeded in a 12-well plate at a density of 1×10^6 cells/well. For CFU-F assay, the cells were

---

old male mice were seeded in 6-well plate at 4×10^5 cells per well. Pip5k1c was knocked down by RNA interference for 48 h. Protein extracts isolated from the cells were subjected to Western blotting with the indicated antibodies (*F*). Gapdh protein were used as internal controls for western blotting analysis. Quantification results (*G*) were expressed as mean ± SD; N = 3 biologically independent experiments. **$p < 0.01$ *versus* si NC; unpaired two-tailed *t* test. *H*, IHC staining. Tibial sections of control and cKO mice were subjected to IHC staining for expression of Runx2. Scale bar, 50 μm. *I*, quantification of (*H*). Results were expressed as mean ± SD; N = 6 mice per group were analyzed. **$p < 0.01$ *versus* control; unpaired two-tailed *t* test. *J* and *K*, tibial sections of control and cKO mice were subjected to IF staining for expression of Osx (*J*). Scale bar, 50 μm. (*K*) quantification of (*J*). Results were expressed as mean ± SD; N = 6 mice per group were analyzed. **$p < 0.01$ *versus* control; unpaired two-tailed *t* test. *L–O*, Flag-Runx2 plasmid (1 μg) was transfected into COS-7 cells together with increasing amounts of plasmids expressing a kinase-dead CaMK2α-V5 (KD-CaMK2α-V5) (*L* and *M*) or constitutively active CaMK2α-V5 (CA-CaMK2α-V5) (*N* and *O*) plasmid. Runx2 expression was determined by Western blotting with anti-Flag antibody at 24 h after transfection. Results were expressed as mean ± SD; N = 3 biologically independent experiments. **$p < 0.01$ *versus* 2 μg; unpaired two-tailed *t* test. *P* and *Q*, cycloheximide experiments. Flad-Runx2 plasmid was transfected into COS-7 cells together with KD-CaMK2α-V5 or CA-CaMK2α-V5 plasmid. At 24 h after transfection, cells were treated with CHX at 100 μg/ml for the indicated times. Quantification of levels of Runx2 protein was performed (*Q*). Results were expressed as mean ± SD; N = 3 biologically independent experiments. **$p < 0.01$ *versus* control; unpaired two-tailed *t* test. si-NC, control siRNA; CA-CaMK2α, constitutively active form of CaMK2α; CHX, cycloheximide; BMSCs, bone marrow stromal cells; IHC, immunohistochemical.
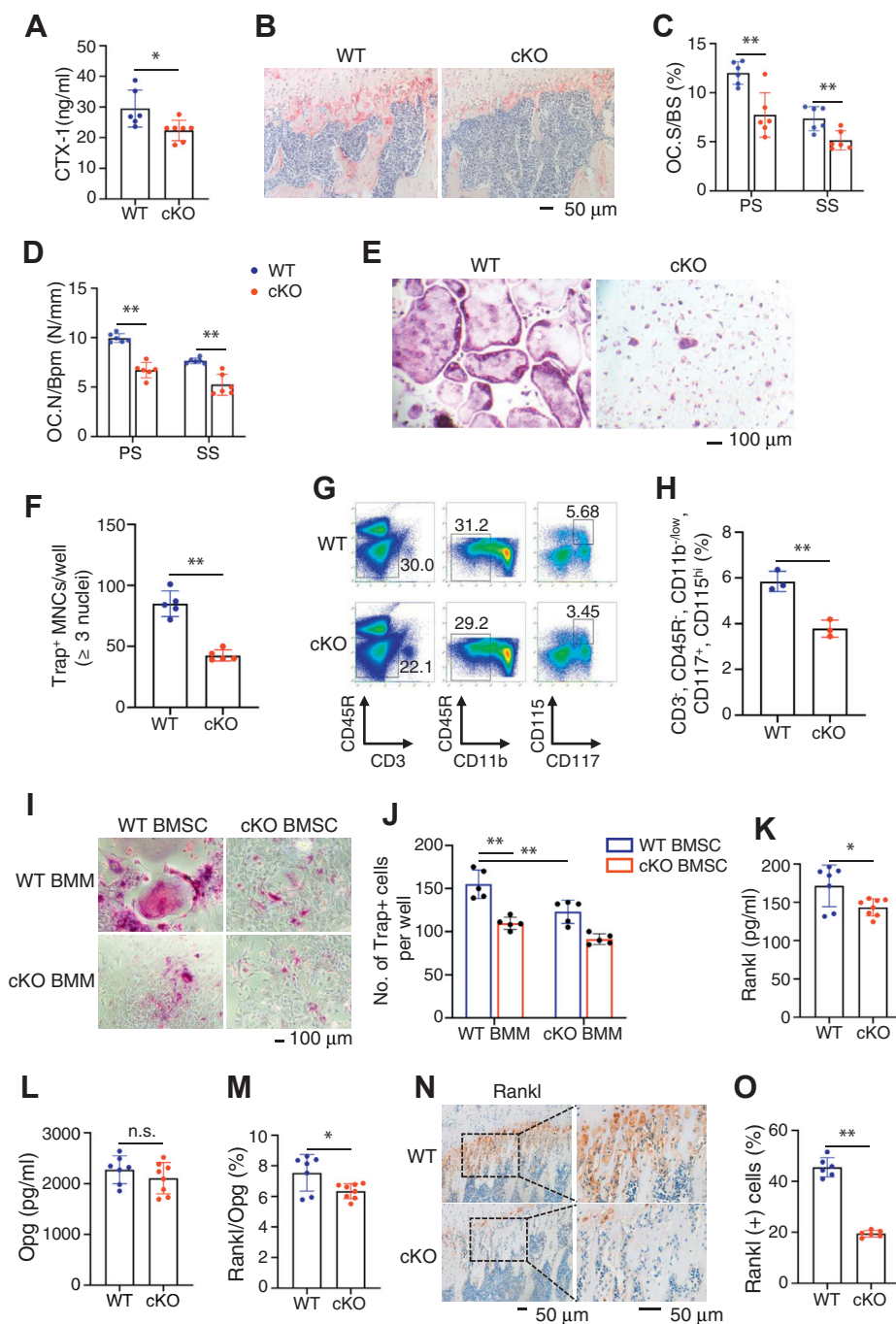
Figure 6. Pip5k1c loss impairs osteoclast formation and bone resorption. *A,* serum levels of collagen type I cross-linked C-telopeptide (CTX-1) from 4-month-old control and cKO male mice. Results were expressed as mean ± SD; $N = 6$ mice for control, $N = 7$ mice for cKO. *$p < 0.05$ *versus* control, Unpaired two-tailed *t* test; *B,* TRAP staining of tibial sections from 4-month-old male mice. Scale bar, 50 μm. *C* and *D,* quantitative analyses of the osteoclast surface per bone surface (*C*) and osteoclast numbers per bone perimeter (*D*) of primary spongiosa (PS) and secondary spongiosa (SS) from (*B*). Results were expressed as mean ± SD; $N = 6$ mice per group from 4-month-old male mice, *$p < 0.05$ *versus* control, unpaired two-tailed *t* test. *E,* bone marrow monocytes (BMMs) from 4-month-old male control (WT) and cKO mice were cultured in osteoclast proliferation medium (α-MEM, 20% FBS +10 ng/ml M-CSF) for 3 days and osteoclast differentiation medium (α-MEM + 20% FBS, 10 ng/ml M-CSF, 50 ng/ml RANKL) for 6 days, followed by TRAP staining. Scale bar, 100 μm. *F,* quantitative analyses of TRAP^{+} multinucleated cells (MNC, defined as having three or more nuclei per cell) generated by each group. Results were expressed as mean ± SD; **$p < 0.01$ *versus* control, unpaired two-tailed *t* test. *G* and *H,* flow cytometry. Bone marrow cells from 4-month-old control and cKO male mice were stained with CD3-FITC, CD45R-PE, CD11b-APC-Cy7, CD117-Percp-Cy5.5, and CD115-APC antibodies and analyzed with flow cytometry as described in Methods. The CD3^{-} CD45R^{-} CD11b^{-/low} CD117^{+} CD115^{hi} cells in bone marrow cells were gated (*G*) and calculated (*H*). Results were expressed as mean ± SD; $N = 3$ male mice per group. **$p < 0.01$ *versus* WT, unpaired two-tailed *t* test. *I* and *J,* BMSC (bone marrow stromal cell)-BMM (bone marrow cell) co-cultures. Primary BMSC and BMM from 4-month-old control and cKO male mice were co-cultured for 14 days in the absence of M-CSF and RANKL, followed by TRAP staining (*I*) and quantitative analyses of TRAP^{+} cells (*J*). Results were expressed as mean ± SD; $N =$ five mice per group. **$p < 0.01$; two-way ANOVA (interaction: F (1,16) =1.744, $p = 0.2053$; Row factor: F (1,16) = 23.07, $p = 0.0002$; column factor: F (1,16) = 54.28, $p < 0.0001$). *K–M,* ELISA assay. Serum levels of Rankl (*K*) and Opg (*L*) from 4-month-old control and cKO male mice were determined. The Rankl/Opg ratio was calculated (*M*). Results were expressed as mean ± SD; $N = 7$ mice for control, $N = 8$ for cKO. *$p < 0.05$ *versus* control, n.s., not significant; unpaired two-tailed *t* test. *N* and *O,* IHC staining. Tibial sections of 4-month-old control and cKO male mice were subjected to IHC staining for expression of Rankl. Scale bar, 50 μm. Quantification data (*O*).

cultured in the Mouse MesenCult proliferation medium (STEMCELL Technologies, cat# 05513) for 14 days, followed by Giemsa staining according to the manufacturer's instruction (Sigma, GS500). For CFU-OB assay, the cells were cultured in differentiation medium (α-MEM containing 10% fetal bovine serum (FBS) and 50 µg/ml L-ascorbic acid and 2 mM β-glycerophosphate) for 21 days, followed by alizarin red staining.

In vitro *osteoblastic and adipogenic differentiation of BMSCs*

Primary BMSCs were isolated from femurs and tibias of 4-month-old male mice and cultured as previously described (28). BMSCs were seeded in 6-well plate at a density of 5×10^5 cells/well and cultured in osteogenic medium (α-MEM containing 10% FBS and 50 µg/ml ascorbic acid) for 7 days followed by qPCR analysis or changed to mineralization-inducing medium (osteogenic medium plus 2.5 mM β-glycerophosphate) for another 7 days, followed by alizarin red S staining (40 mM, pH 4.2) (Sigma). *In vitro* adipogenic differentiation was performed as we previously described (29). Briefly, primary BMSCs were isolated from 4-month-old male control and cKO mice and cultured with adipogenic medium for 7 days, followed by RT-qPCR analyses, or for 14 days, followed by oil red O staining.

Osteoclast assays

Tibial sections were used for TRAP staining for evaluation of *in vivo* osteoclast formation and was performed as we previously described (30). BMMs were used for the *in vitro* osteoclast differentiation assay as we previously described (31). Co-culture experiments were performed as we previously described (30). Briefly, primary BMSCs were seeded in a 24-well plate, and BMMs were seeded on the top of BMSCs. These cells were cultured for 14 days in α-MEM containing 10% FBS, 10^{-8} M dexamethasone, and 10^{-8} M 1,25 dihydroxyvitamin D3. TRAP$^+$ MNCs were scored.

Serum ELISA assay

ELISA assay was conducted as we previously described (29). Briefly, blood samples were collected from WT and cKO mice. Serum P1NP, CTX-1, Rankl, and Opg were measured by using P1NP ELISA kit (Immunodiagnostic Systems Limited, cat# AC-33F1), CTX-1 ELISA kit (Immunodiagnostic Systems Limited, cat# AC-06F1), Rankl ELISA kit (R&D, cat# MTR00), and Opg ELISA kit (R&D, cat# MOP00), respectively, according to the manufacturers' instructions.

Flow cytometry

Flow cytometry was conducted as we did before (30). Briefly, BM cells were flushed out from 2-month-old male mice femurs. After erythrocytes were removed by lysis, BMM cells were washed, scored, and resuspended at a density of 5 x

10^6 cells/ml in cold PBS containing 2% FBS. Fluorescent conjugate antibodies were used to stain the BMMs. Antibodies against CD3-FITC (eBioscience, cat# 11-0032-82, 1:200), CD45R-PE (eBioscience, cat# 12-0452-82, 1:200), CD11b-APC-Cy7 (BD Biosciences, cat# 561039, 1:200), CD117-Percp-Cy5.5 (BD Biosciences, cat# 560557, 1:200), and CD115-APC (eBioscience, cat# 17-1152-82, 1:200) were used to stain BMMs at 4 °C for 45 min. Then BMMs were washed with ice-cold PBS containing 2% FBS for 3 times. Finally, cells were collected and resuspended in 500 µl ice-cold PBS followed by analysis with a flow cytometer (BD Biosciences). Data were processed with FlowJo Software (Becton, Dickinson and Company).

siRNA and plasmid

The negative control and mouse-specific *Pip5k1c* siRNAs used in this study were synthesized by Suzhou GenePharma Co., Ltd (Suzhuo, China). Mouse negative control siRNA sequence: 5′-UUCUCCGAACGUGUCACGUTT-3′, Mouse *Pip5k1c* siRNA sequence: 5′-GCUUCUAUGCAGAGC GCUUTT-3′, the Flag-Runx2, V5-KD CaMK2α (K42R), and V5-CA CaMK2α (T286D) constructs were purchased from Guangzhou IGE Biotechnology, Ltd.

Cell culture and transfection

Primary BMSCs were isolated from 4-month-old male mice and cultured in α-MEM containing 20% FBS. COS-7 cells were cultured in Dulbecco's modified Eagle's medium containing 10% FBS. Transient transfection was conducted when cells reached to 80% confluence with specific siRNAs using lipofectamine RNAiMAX transfection reagent (Invitrogen, cat# 13778150) and plasmids using lipofectamine 3000 transfection reagent (Invitrogen, cat# L3000015) according to the manufacturers' protocols as we previously described (32).

Cytosol Ca^{2+} assay

The Ca^{2+}-sensitive fluorescent dye Fluo-4/AM (Yeasen) was used to detect cytoplasmic Ca^{2+} levels. Briefly, BMSCs seeded in confocal dish were washed twice with D-Hank's buffer and incubated with 5 µM Fluo-4/AM at 37 °C for 30 min away from light. Then, the cells were washed three times with D-Hank's buffer and further incubated with D-Hank's buffer at 37 °C for another 30 min. Finally, signals were collected with a confocal laser scanning microscope (Leica SP8) using a ×20 objective lens at 488 nm. The cytoplasmic Ca^{2+} concentrations were recorded as total fluorescence intensity. The fluorescence intensity variation was recorded from cells.

Real-time quantitative reverse transcription PCR analyses

RNA isolation, reverse transcription, and qPCR analyses were conducted as previously described (20). DNA sequences of mouse primers used for qPCR analyses for expression of the

---

following genes were as follows: Gapdh: up 5′-CAGTGCC AGCCTCGTCCCGTAGA-3′, down 5′-CTGCAAATGGCAG CCCTGGTGAC-3′; Pip5k1c: up 5′-GGATGCGTCGGGAGA GACTA-3′, down 5′-AGGTCTTGAAGCGGAAATCCT-3′; Runx2: up 5′-AACGATCTGAGATTTGTGGGC, down 5′-CC TGCGTGGGATTTCTTGGTT-3′; Osx: up 5′-ATGGC GTCCTCTCTGCTTG-3′, down 5′-TGAAAGGTCAGCGTA TGGCTT-3′; Col1α1: up 5′-GCTCCTCTTAGGGGCCA CT-3′, down 5′-CCACGTCTCACCATTGGGG-3′; Alp: up 5′-CCAACTCTTTTGTGCCAGAGA-3′, down 5′-GGCTAC ATTGGTGTTGAGCTTTT-3′; Ocn: up 5′-AGGGAGG ATCAAGTCCCG-3′, down 5′-GAACAGACTCCGGCG CTA-3′; Pref-1: up 5′-CCCAGGTGAGCTTCGAGTG-3′, down 5′-GGAGAGGGGTACTCTTGTTGAG-3′; Pparγ2: up 5′-TCGCTGATGCACTGCCTATG-3′, down 5′-GAGAGG TCCACAGAGCTGATT-3′; Cebp/α: up 5′-CAAGAACAGC AACGAGTACCG-3′, down 5′-GTCACTGGTCAACTCCA GCAC-3′; Cebp/β: up 5′-CAAGCTGAGCGACGAGTACA-3′, down 5′-CAGCTGCTCCACCTTCTTCT-3′; Ap2: up 5′-GGGGCCAGGCTTCTATTCC-3′, down 5′-GGAGC TGGGTTAGGTATGGG-3′; and Adiponectin: up 5′-TGTT CCTCTTAATCCTGCCCA-3′, down 5′-CCAACCTGCACAA GTTCCCTT-3′.

Western blot analyses

Protein isolation and Western blot analyses were performed as we previously described (26). The antibodies against the following proteins for western blotting analyses were as follows: Gapdh (ZSGB-BIO, cat# TA-08, 1:1000); Pip5k1c (Cell Signaling Technology, cat# 3296, 1:1000); Runx2 (Cell Signaling Technology, cat# 12556, 1:1000); Flag (Sigma, cat# F1804, 1:1000); V5 (Invitrogen, cat# R960-25, 1:1000). CaMK2 (pan) (Cell Signaling Technology, cat# 4436, 1:1000); p-CaMK2 (T286) (Cell Signaling Technology, cat# 12716, 1:1000); Erk ½ (Cell Signaling Technology, cat# 9102, 1:1000); p-Erk ½ (Cell Signaling Technology, cat# 9101, 1:1000); Creb (Cell Signaling Technology, cat# 9197, 1:1000); p-Creb (Cell Signaling Technology, cat# 9198, 1:1000); active β-catenin (Cell Signaling Technology, cat# 8814, 1:1000); and total β-catenin (Cell Signaling Technology, cat# 4270, 1:1000).

IHC staining

IHC staining was performed on 5-μm paraffin sections of the decalcified tibiae with the indicated antibodies using the Envision System-HRP (DAB) kit (DAKO North America, Inc.) following the standard protocols as described previously (20). The antibodies against the following proteins for IHC in this project were as follows: Runx2 (Abcam, cat# ab192256, 1:1000); Osx (Abcam, cat# ab22552, 1:1000); and Rankl (Santa Cruz, cat# SC-9073, 1:1000).

Immunofluorescence staining

Immunofluorescence staining was performed as previously described (32) on 5-μm paraffin sections of the decalcified tibiae. Briefly, the sections were dewaxed with xylene and rehydrated with 100% ethyl alcohol, 95% ethyl alcohol, 70%

ethyl alcohol, and PBS. Sections were then performed antigen retrieval with citrate buffer (pH6.8) and incubated with immunostaining permeabilization solution with saponin (Beyotime, cat# P0095) for 10 min, and blocked with immunol staining blocking buffer (Beyotime, cat# P0102) for 1 h at room temperature. Following that, the Ocn (Bioss Antibodies, cat# BS-4917R) antibody was diluted into the primary antibody dilution buffer (Beyotime, cat# P0262) with 1:300 ratio, and the sections were incubated with the diluted primary antibody for overnight at 4 °C. Sections were washed with 1x PBS for 3 times and incubated with goat anti-rabbit alexa fluor 488 secondary antibody (Invitrogen, cat# A11008) diluted by secondary antibody dilution buffer (Beyotime, cat# P0265) at room temperature for 1 h. The sections were washed with 1 × PBS for 3 times and immediately mounted with mounting medium with DAPI (Abcam, cat# ab104139). The Ocn signal was acquired with Nikon Confocal A1R system under 20x objective lens.

Statistics

Mice used in experiments of this study were randomly grouped. IF, IHC, and histology were conducted and analyzed in a double-blinded way. Statistical analyses were performed using the GraphPad Prism 8. The two-tailed unpaired Student's t test (two groups) and two-way ANOVA (multiple groups), followed by Tukey's post-hoc test, were used. Results are expressed as mean ± standard deviation, as indicated in the Figure Legends. Differences with $p < 0.05$ were considered statistically significant.

Data availability

All data are available from the corresponding author upon reasonable request.

dependent protein kinase; CA-CaMK2α, constitutively active form of CaMK2α; CFU-F, colony forming unit-fibroblast; CFU-OB, colony forming unit-osteoblast; CTX-1, collagen type 1 cross-linked C-telopeptide; ER, endoplasmic reticulum; FBS, fetal bovine serum; IHC, immunohistochemical; IP3, inositol 1,4,5 trisphosphate; KD, knockdown; MNCs, multinucleated cells; μCT, microcomputed tomography; MAR, mineral apposition rate; MSC, mesenchymal stem cell; MS/BS, mineralizing surface per bone surface; Ocn, osteocalcin; opg, osteoprotegerin; Pip5k1c, phosphatidylinositol-4-phosphate 5-kinase type-1 gamma; P1NP, procollagen type 1 amino terminal propeptide; Rankl, receptor activator of nuclear factor-κB ligand; Tb.N, trabecular number; Tb.Sp, trabecular separation; Tb.Th, trabecular thickness.

References

1. Ishihara, H., Shibasaki, Y., Kizuki, N., Wada, T., Yazaki, Y., Asano, T., and Oka, Y. (1998) Type I phosphatidylinositol-4-phosphate 5-kinases. Cloning of the third isoform and deletion/substitution analysis of members of this novel lipid kinase family. *J. Biol. Chem.* **273**, 8741–8748

2. Di Paolo, G., Moskowitz, H. S., Gipson, K., Wenk, M. R., Voronov, S., Obayashi, M., Flavell, R., Fitzsimonds, R. M., Ryan, T. A., and De Camilli, P. (2004) Impaired PtdIns(4,5)P2 synthesis in nerve terminals produces defects in synaptic vesicle trafficking. *Nature* **431**, 415–422

3. Legate, K. R., Montag, D., Bottcher, R. T., Takahashi, S., and Fassler, R. (2012) Comparative phenotypic analysis of the two major splice isoforms of phosphatidylinositol phosphate kinase type Igamma *in vivo*. *J. Cell Sci.* **125**, 5636–5646

4. Ling, K., Doughman, R. L., Firestone, A. J., Bunce, M. W., and Anderson, R. A. (2002) Type I gamma phosphatidylinositol phosphate kinase targets and regulates focal adhesions. *Nature* **420**, 89–93

5. Unoki, T., Matsuda, S., Kakegawa, W., Van, N. T., Kohda, K., Suzuki, A., Funakoshi, Y., Hasegawa, H., Yuzaki, M., and Kanaho, Y. (2012) NMDA receptor-mediated PIP5K activation to produce PI(4,5)P(2) is essential for AMPA receptor endocytosis during LTD. *Neuron* **73**, 135–148

6. van den Bout, I., and Divecha, N. (2009) PIP5K-driven PtdIns(4,5)P2 synthesis: Regulation and cellular functions. *J. Cell Sci.* **122**, 3837–3850

7. Vasudevan, L., Jeromin, A., Volpicelli-Daley, L., De Camilli, P., Holowka, D., and Baird, B. (2009) The beta- and gamma-isoforms of type I PIP5K regulate distinct stages of Ca2+ signaling in mast cells. *J. Cell Sci.* **122**, 2567–2574

8. Volpicelli-Daley, L. A., Lucast, L., Gong, L. W., Liu, L., Sasaki, J., Sasaki, T., Abrams, C. S., Kanaho, Y., and De Camilli, P. (2010) Phosphatidylinositol-4-phosphate 5-kinases and phosphatidylinositol 4,5-bisphosphate synthesis in the brain. *J. Biol. Chem.* **285**, 28708–28714

9. Wang, Y. J., Li, W. H., Wang, J., Xu, K., Dong, P., Luo, X., and Yin, H. L. (2004) Critical role of PIP5KI{gamma}87 in InsP3-mediated Ca(2+) signaling. *J. Cell Biol.* **167**, 1005–1010

10. Wang, Y., Lian, L., Golden, J. A., Morrisey, E. E., and Abrams, C. S. (2007) PIP5KI gamma is required for cardiovascular and neuronal development. *Proc. Natl. Acad. Sci. U. S. A.* **104**, 11748–11753

11. Yu, Y. L., Chou, R. H., Chen, L. T., Shyu, W. C., Hsieh, S. C., Wu, C. S., Zeng, H. J., Yeh, S. P., Yang, D. M., Hung, S. C., and Hung, M. C. (2011) EZH2 regulates neuronal differentiation of mesenchymal stem cells through PIP5K1C-dependent calcium signaling. *J. Biol. Chem.* **286**, 9657–9667

12. Zhu, T., Chappel, J. C., Hsu, F. F., Turk, J., Aurora, R., Hyrc, K., De Camilli, P., Broekelmann, T. J., Mecham, R. P., Teitelbaum, S. L., and Zou, W. (2013) Type I phosphotidylinositol 4-phosphate 5-kinase gamma regulates osteoclasts in a bifunctional manner. *J. Biol. Chem.* **288**, 5268–5277

13. Boyle, W. J., Simonet, W. S., and Lacey, D. L. (2003) Osteoclast differentiation and activation. *Nature* **423**, 337–342

14. Zhou, B. O., Yue, R., Murphy, M. M., Peyer, J. G., and Morrison, S. J. (2014) Leptin-receptor-expressing mesenchymal stromal cells represent the main source of bone formed by adult bone marrow. *Cell Stem Cell* **15**, 154–168

15. Long, F. (2012) Building strong bones: Molecular regulation of the osteoblast lineage. *Nat. Rev. Mol. Cell Biol.* **13**, 27–38

16. Harada, S., and Rodan, G. A. (2003) Control of osteoblast function and regulation of bone mass. *Nature* **423**, 349–355

17. Zayzafoon, M. (2006) Calcium/calmodulin signaling controls osteoblast growth and differentiation. *J. Cell. Biochem.* **97**, 56–70

18. Vimalraj, S., Arumugam, B., Miranda, P. J., and Selvamurugan, N. (2015) Runx2: Structure, function, and phosphorylation in osteoblast differentiation. *Int. J. Biol. Macromol.* **78**, 202–208

19. Logan, M., Martin, J. F., Nagy, A., Lobe, C., Olson, E. N., and Tabin, C. J. (2002) Expression of Cre Recombinase in the developing mouse limb bud driven by a Prxl enhancer. *Genesis* **33**, 77–80

20. Zhu, K., Lai, Y., Cao, H., Bai, X., Liu, C., Yan, Q., Ma, L., Chen, D., Kanaporis, G., Wang, J., Li, L., Cheng, T., Wang, Y., Wu, C., and Xiao, G. (2020) Kindlin-2 modulates MafA and beta-catenin expression to regulate beta-cell function and mass in mice. *Nat. Commun.* **11**, 484

21. Jacquin, C., Gran, D. E., Lee, S. K., Lorenzo, J. A., and Aguila, H. L. (2006) Identification of multiple osteoclast precursor populations in murine bone marrow. *J. Bone Miner. Res.* **21**, 67–77

22. Huang, J., Zhao, L., Fan, Y., Liao, L., Ma, P. X., Xiao, G., and Chen, D. (2019) The microRNAs miR-204 and miR-211 maintain joint homeostasis and protect against osteoarthritis progression. *Nat. Commun.* **10**, 2876

23. Wu, C., Jiao, H., Lai, Y., Zheng, W., Chen, K., Qu, H., Deng, W., Song, P., Zhu, K., Cao, H., Galson, D. L., Fan, J., Im, H. J., Liu, Y., Chen, J., *et al.* (2015) Kindlin-2 controls TGF-beta signalling and Sox9 expression to regulate chondrogenesis. *Nat. Commun.* **6**, 7531

24. Bouxsein, M. L., Boyd, S. K., Christiansen, B. A., Guldberg, R. E., Jepsen, K. J., and Muller, R. (2010) Guidelines for assessment of bone microstructure in rodents using micro-computed tomography. *J. Bone Miner. Res.* **25**, 1468–1486

25. Cao, H., Yan, Q., Wang, D., Lai, Y., Zhou, B., Zhang, Q., Jin, W., Lin, S., Lei, Y., Ma, L., Guo, Y., Wang, Y., Wang, Y., Bai, X., Liu, C., *et al.* (2020) Focal adhesion protein Kindlin-2 regulates bone homeostasis in mice. *Bone Res.* **8**, 2

26. Zhu, K., Yi, J., Xiao, Y., Lai, Y., Song, P., Zheng, W., Jiao, H., Fan, J., Wu, C., Chen, D., Zhou, J., and Xiao, G. (2015) Impaired bone homeostasis in amyotrophic lateral sclerosis mice with muscle atrophy. *J. Biol. Chem.* **290**, 8081–8094

27. Yu, S., Zhu, K., Lai, Y., Zhao, Z., Fan, J., Im, H. J., Chen, D., and Xiao, G. (2013) ATF4 promotes beta-catenin expression and osteoblastic differentiation of bone marrow mesenchymal stem cells. *Int. J. Biol. Sci.* **9**, 256–266

28. Lei, Y., Fu, X., Li, P., Lin, S., Yan, Q., Lai, Y., Liu, X., Wang, Y., Bai, X., Liu, C., Chen, D., Zou, X., Cao, X., Cao, H., and Xiao, G. (2020) LIM domain proteins Pinch1/2 regulate chondrogenesis and bone mass in mice. *Bone Res.* **8**, 37

29. Wang, Y., Yan, Q., Zhao, Y., Liu, X., Lin, S., Zhang, P., Ma, L., Lai, Y., Bai, X., Liu, C., Wu, C., Feng, J. Q., Chen, D., Cao, H., and Xiao, G. (2019) Focal adhesion proteins Pinch1 and Pinch2 regulate bone homeostasis in mice. *JCI Insight* **4**, e131692

30. Cao, H., Yu, S., Yao, Z., Galson, D. L., Jiang, Y., Zhang, X., Fan, J., Lu, B., Guan, Y., Luo, M., Lai, Y., Zhu, Y., Kurihara, N., Patrene, K., Roodman, G. D., *et al.* (2010) Activating transcription factor 4 regulates osteoclast differentiation in mice. *J. Clin. Invest.* **120**, 2755–2766

31. Cao, H., Zhu, K., Qiu, L., Li, S., Niu, H., Hao, M., Yang, S., Zhao, Z., Lai, Y., Anderson, J. L., Fan, J., Im, H. J., Chen, D., Roodman, G. D., and Xiao, G. (2013) Critical role of AKT protein in myeloma-induced osteoclast formation and osteolysis. *J. Biol. Chem.* **288**, 30399–30410

32. Fu, X., Zhou, B., Yan, Q., Tao, C., Qin, L., Wu, X., Lin, S., Chen, S., Lai, Y., Zou, X., Shao, Z., Wang, M., Chen, D., Jin, W., Song, Y., *et al.* (2020) Kindlin-2 regulates skeletal homeostasis by modulating PTH1R in mice. *Signal Transduct Target Ther.* **5**, 297